Available online at www.sciencedirect.com
ScienceDirect
Experimental Thermal and Fluid Science 32 (2007) 262–275
Experimental Thermal and Fluid Science
www.elsevier.com/locate/etfs

Particle image velocimetry measurements for opposing flow in a vertical channel with a differential and asymmetric heating condition

L. Martínez-Suástegui [a,*], C. Treviño [b,1]

[a] Graduate Student, Facultad de Ingeniería, Universidad Nacional Autónoma de México, C.U., México 04510 D.F., Mexico
[b] Facultad de Ciencias, Universidad Nacional Autónoma de México, C.U., México 04510 D.F., Mexico

Received 29 January 2007; accepted 10 April 2007

Abstract

Particle image velocimetry (PIV) measurements were carried out in an experimental investigation of laminar mixed convection in a vertical duct with a square cross-section. The main downward water-flow is driven by gravity while a portion of a lateral side is heated, and buoyancy forces produce non-stationary vortex structures close to the heated region. Various ranges of the Grashof number, Gr are studied in combination with the Reynolds number, Re varying from 300 to 700. The values of the generalized buoyancy parameter or Richardson number, $Ri = Gr/Re^2$ parallel to the Grashof number are included in the results. The influence of these nondimensional parameters and how they affect the fluid flow structure and vortex sizes and locations are reported. The flow patterns are nonsymmetric, periodic, and exhibit increasing complexity and frequency for increasing buoyancy. For the averaged values of the resulting vortex dimensions, it was found that a better and more congruent representation occurs when employing the Grashof and Reynolds numbers as independent parameters.

PACS: 44.25.+f; 47.55.P−; 47.15.−x

Keywords: Mixed convection; Opposed flows; PIV; Unsteady convective flows

1. Introduction

Buoyant effects in fluid flow in channels have been studied extensively due to its practical applications including the design of compact heat exchangers, solar collectors, nuclear reactors and the cooling of electronic equipment. The subject of forced and mixed convection in rectangular ducts with uniform heating conditions has been widely treated in the literature, as can be seen in the review on this subject by Hartnett and Kostic [1]. Thermal buoyancy forces play a significant role in forced convection heat transfer when the flow velocity is relatively small and the temperature difference between the surface and the free stream is relatively large. The thermal buoyancy force may be either assisting or opposing the forced flow, depending on the forced flow direction relative to gravity and the heating/cooling conditions. Mixed convection is in general a multi-parametric process. Together with the geometrical parameters arising in any specific problem, there are three important parameters. The Reynolds (Re), Grashof (Gr) and Prandtl (Pr) numbers characterize the forced flow and the influence of buoyancy. However, depending on the specific problem studied, instead of using the Reynolds and Grashof numbers as independent parameters, a combination of the form Gr/Re^n is frequently employed in addition to the Reynolds number. The value of $n = 2$ is used by simple reasons. The order of magnitude

* Corresponding author. Tel.: +52 55 56224854; fax: +52 55 56160326.
E-mail address: martinezlorenzo@gmail.com (L. Martínez-Suástegui).
[1] On sabbatical leave at Institute of Chemistry, ELTE Budapest, Hungary.

0894-1777/$ - see front matter © 2007 Elsevier Inc. All rights reserved.
doi:10.1016/j.expthermflusci.2007.04.003

Nomenclature

g	gravity acceleration
f	frequency (Hertz)
Gr	Grashof number based on channel width, $Gr = g\beta(T_w - T_0)H^3/\nu^2$
H	channel width
L_1	length from the inlet to the heated slab (see Fig. 2)
L_2	length of the heated slab (see Fig. 2)
L_3	length from the heated slab to the channel outlet (see Fig. 2)
N	number of spatial points in the domain
Re	Reynolds number based on channel width, $Re = U_0H/\nu$
Ri	Richardson number based on channel width, $Ri = Gr/Re^2$
St	Strouhal number, $St = fH/U_0$
t	time
t_f	final measuring time
U_0	free stream velocity
U,V	velocity components in x- and y-directions (see Fig. 2)
x_p	mass flux centroid introduced in Eq. (1)
x, y, z	rectangular Cartesian coordinates
T_0	water temperature at the channel entrance
T_W	averaged temperature in the heated slab
Greeks	
β	volumetric expansion coefficient
ν	kinematic viscosity
ω	instantaneous, out of plane vorticity
ρ	fluid density
Subscript	
i, j	spatial coordinate indices

of the induced Reynolds number caused by buoyancy in the classical problem of boundary layer of a heated vertical plate is related to the square root of the Grashof number. The study by Aung and Worku [2] provided theoretical results for mixed convection flows between parallel plate channels with unequal wall temperatures and showed that when the parameter Gr/Re exceeds a certain threshold value, flow reversal occurs. In further studies for vertically upward flow in a parallel plate channel, the same authors [3] presented criteria for the occurrence of flow reversal and showed that buoyancy dramatically increases the hydrodynamic development length and diminishes the thermal development distance. Ingham et al. [4] obtained solutions to combined convection flows in a vertical parallel plate duct with asymmetric wall temperature boundary conditions and presented the whole development of the flow for situations when flow reversal occurs. They also obtained a new value of Gr/Re for the onset of flow reversal. Evans and Greif [5] studied numerically the downward flow of nitrogen in a tall, partially heated vertical channel, showing the strong effects of buoyancy even for small temperature differences and reporting time dependant oscillations including periodic flow reversals along the channel walls. Lin et al. [6] studied the unsteady laminar aiding and opposing mixed convection heat transfer in a vertical flat duct for an initially fully developed flow proposing correlation equations for the time variations of the local Nusselt numbers. Yao [7] obtained an analytical solution for the fluid flow and the heat transfer in the entry region of a heated vertical channel for constant wall temperature and constant wall heat flux conditions, suggesting that moving periodic and recirculating cells are generated if natural convection is a dominant mode. Chang and Lin [8] performed numerical studies on the steady laminar and transient oscillatory mixed convection of a low Prandtl number fluid in a symmetrically heated vertical plane channel subject to an opposing buoyancy by solving the transient two-dimensional flow and energy equations. The authors carried out a linear stability analysis by assuming an infinite heated section and found that an oscillatory flow with a single fundamental frequency is found when the buoyancy parameter or Richardson number, which is a function of the Reynolds number, exceeds a critical value. Epildorou et al. [9] obtained numerical results for two-dimensional, steady aiding mixed convection from a vertical channel with adiabatic walls having a flush-mounted, isoflux heat source on one of the walls, pointing that the strength and extent of the convective cells strongly depend on the value of the Grashof and Reynolds numbers. Lin et al. [10] studied numerically the flow and thermal characteristics in transient laminar opposing mixed convection in a vertical plane channel subject to a symmetric heat input. Their results show that at high opposing buoyancy, sudden flow asymmetry and oscillation occur simultaneously in a nearly steady flow after an initial transient, noting periodic flow and thermal evolution in space and time. Sparrow et al. [11] made experimental measurements with water for natural convection in a one-sided heated vertical channel and reported the apparition of a recirculation pocket. Zhang and Dutta [12] made experimental measurements and analysis on buoyancy-assisted mixed convection in a vertical square channel with asymmetric conditions by using four different heating configurations varying the Reynolds number and buoyancy parameter Gr/Re^2, concluding that the local heat transfer coefficient increases with increasing buoyancy parameter. Experimental investigations of laminar mixed convection flow have been made by Odouza et al. [13], Kimura et al. [14], Abu-Mulaweh [15], Gau et al. [16] and Wirtz and Stutzman [17]. Unfortunately, all of the experimental investigations focus on the

overall plate heat transfer and neglect flow structure and dynamics of this relatively simple, laminar flow. However, the correct and direct identification and observation of vortical structures and their interactions in the flow has received little attention to date. Techniques with single point measurements, such as hot wires, surface pressure sensors and laser Doppler anemometry (LDA) are very useful for analyzing the statistical data of the flow. Unfortunately, the physical structures in laminar mixed convection opposing flow and their dynamics have been difficult to investigate with these techniques because of the difficulty involved in obtaining multi-point measurements with high spatial resolution instantaneously throughout the flow domain. The aim of this investigation is to conduct a detailed experimental study (using PIV) of the instantaneous flow structure and evolving dynamics of flow reversal in a mixed convection flow. Two-dimensional (2D), spatio-temporal measurements of velocity and vorticity in the x–y and x–z planes are made. Flow visualization images are also presented to support the PIV data. As a result, non-intrusive and instantaneous 2D measurements with higher spatial resolution than arrays of single point measurement probes are achieved over a relatively large region of the flow.

2. Instrumentation and experimental facility

The schematic diagram of the experimental setup of the water-flow channel is shown in Fig. 1. Water enters through the upper opening of a vertical square duct of width $H = 67$ mm and 700 mm long with a uniform velocity U_0. Gravity moves the flow down, and flow uniformity is achieved with flow rectifiers that are mounted both at the channel entrance and at the exit of the test section. Velocity measurements in the free stream at the channel entrance show that the free stream velocity is uniform and constant, and the repeatability of the mean measurements is estimated around 1%. The channel walls are 10 mm thick and are made of Plexiglass (acrylic) with an aluminum heated slab with uniform temperature T_W located at the midheight on one of the side walls. The slab has a length of $L_2 = 80$ mm and is 70 mm wide, thus occupying the whole channel depth. The surface temperature of the slab is measured with 9 thermocouples epoxied on the back of the slab at regular intervals along its area. The average of the nine readings is taken for the slab's temperature, and the temperature gradient in the longitudinal direction of the slab has a maximum value of 0.00025 K/mm. The slab is heated from outside by a commercial electric strip heater immersed in a secondary water deposit, and the input energy is determined by measuring the current and the voltage drop across the electric strip. The uncertainty associated with the energy input as determined from these measurements is less than 2%. By monitoring the local temperature of the heated slab with the imbedded thermocouples, the temperature of the heated surface can be maintained constant and uniform. Conduction heat losses through the acrylic walls are evaluated, and the ratio of the heat losses per unit area to the heat addition at the heated slab per unit area is less than 1%. This value depends on the ratio of thermal conductivities of the acrylic and water and the thickness of the acrylic compared with the length of the heated slab. Due to the fact that the active surface for heat loss has the same order of magnitude than that of the heated slab, the walls can be assumed to be adiabatic from a practical point of view. The flow control is achieved by a feed back flow loop from a centrifugal pump to the tank bypassing the test facility. One prerequisite for the initiation of the experimental measurements is that the temperature of the water at the inlet ceases to increase. The attainment of thermal equilibrium between the water in the storage tank and the water that exits the test section is a matter of time, and it is achieved when the heat provided equals the heat losses in the circuit. The measurements are done when the inlet temperature reaches its equilibrium value after approximately 30 min. The Reynolds, Grashof and Prandtl numbers are computed based on the thermophysical properties evaluated with the arithmetic mean

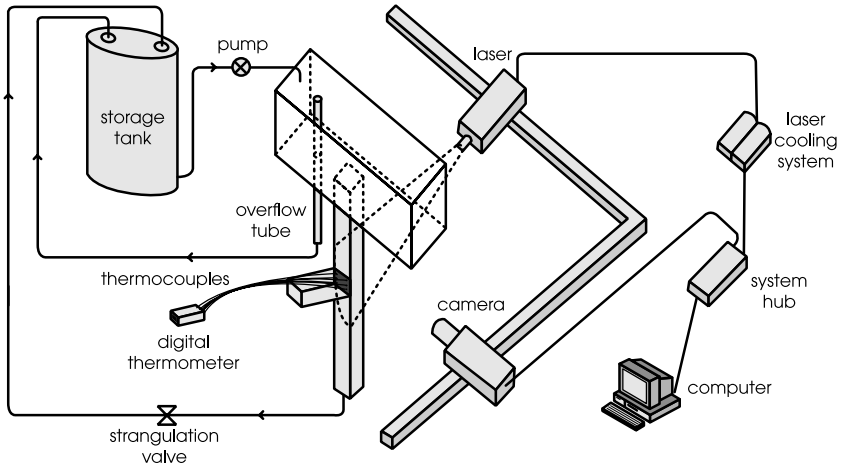

Fig. 1. Experimental setup.

between the slab and the fluid temperature at the inlet. The Reynolds number is varied with a valve that regulates the volume flow rate, which is measured by calibrating water volume in a graduated container and measuring the elapsed time with a stopwatch. As mentioned before in the Introduction Section, the flow behavior depends on three independent nondimensional parameters: The Reynolds, $Re = U_0H/\nu$, and Grashof $Gr = g\beta(T_w - T_0)H^3/\nu^2$ numbers, which take into account the forced and natural convective processes; the Prandtl number relating the viscous and thermal diffusivities of the fluid and a couple of geometrical parameters. In the present experimental setup, the geometrical parameters as well as the Prandtl number are fixed, and only the Grashof and Reynolds numbers are varied. Instead of using the Reynolds and Grashof numbers as the independent parameters, we choose the Reynolds and the Richardson number, $Ri = Gr/Re^2$, as the nondimensional parameters that govern mixed convection. However, due to the fact that the experiments are made by fixing the Reynolds number, a linear dependence of the Grashof and the Richardson numbers is always obtained. For a given Reynolds number, the Richardson number is modified by varying the temperature difference between the slab and the fluid. When $T_W > T_0$, buoyancy opposes the mean forced flow creating flow reversal with an asymmetric velocity profile and generating complex vortex structures appearing in the vicinity of the heated plate. These structures are reported and described in the following section. Uncertainties in results are mostly from the resolutions of measuring devices (instrumental deviation). The uncertainties for the Reynolds and Grashof numbers are 2% and 9%, respectively. A Dantec Dynamics particle image velocimetry system is used to measure the vertical and horizontal velocity components in a plane parallel to the mean flow. The PIV system is equipped with an automated three-dimensional traverse system for positioning the camera and the laser at any desired point in the flow domain. The plane is illuminated by a 120 mJ double pulse Nd:YAG laser (New Wave Gemini) at a wavelength of 532 nm with a duration of the pulsed illumination of 10 ns. The time interval between the two laser pulses is adjusted depending on the value of the Reynolds number, varying from 9000 to 9500 μs. The laser is equipped with a lens system producing a diverging light sheet not exceeding a 1 mm thickness. A Hi Sense, 12 bit camera with 1280×1024 pixels at 8 frames per second is used, and the images are processed using an interrogation window of 64×64 pixels with a 50% vertical and 25% horizontal overlap. The tracer employed is polyamide with a diameter of 20 μm, and seeding density is such that at least 15 particles are contained per interrogation area. Homogeneous and steady seeding is necessary to avoid vector drop out, which increases the possibilities of error in mean and fluctuating velocities. The camera, with an orientation perpendicular to the measuring plane, is fitted with a 60 mm Nikon lens. Velocity vectors are derived from double frame pixel PIV images using an adaptive-correlation algorithm. The test section occupies 98.5% of the whole channel width, and several maps are obtained for different values of the Richardson number. Five data sets with 180 pairs of images are acquired for each location under one flow condition. It was established, through repeated PIV measurements, that 1800 acceptable PIV samples of the local instantaneous fluctuating velocity components are sufficient to repeatedly and accurately determine the local mean velocity in the flow domain. The repeatability of the velocity measurements is within 4%, and the uncertainties in the measured results are estimated (at a 95% confidence level) according to the procedure outlined by Moffat [18]. The longitudinal and transverse velocity as well as the vorticity fields are obtained after statistical evaluation by the PIV processor. The PIV measurement system includes visualization and capture of images, calculation of two-dimensional velocity vectors, and post-processing for analysis. The vector field of the flow velocity within the plane of the light sheet is determined by forming the displacement between the images of the tracer particle and the delay time between the two laser pulses. All of the data acquisition system and major parameters of the working section are shown in Table 1.

The whole length of the channel is divided into a total of eight regions so that the camera is close enough to capture the details of the flow recirculation and not only the large scales of the vortex formations. Each region occupies the whole image size of 1280×1024 pixels and their location with reference names is represented in Fig. 2. The images displayed capture 66 mm out of 67 mm of the channel width, and have a height of 53 mm in the longitudinal direction. Measurements for each vector map in the square duct are taken with y as the longitudinal coordinate (positive upward) and x as the transverse coordinate ($x = 0$ at

Table 1
Parameters used to perform experimental measurements

System	Deionized water
Temperature	298–310 K
Reynolds number	$300 < Re < 700$
Seeding	Polyamide with mean diameter 20 μm and density 1130 kg/m^3
Image size	1280×1024 pixels
Time interval between pulses	9000–9500 μs
Nd:YAG PIV laser	New Wave Gemini, wavelength 532 nm, power 120 mJ/pulse
Pulse-length duration	10 ns
Light pulses per recording	2
Light sheet thickness	≈1 mm
CCD camera	Hi Sense 12 bit, 1280×1024 pixels, double frame mode
Time between two frames	0.01 μs
Frame rate	4 pairs/s
PIV interrogation algorithm	Adaptive-correlation
Interrogation resolution	64×64 pixels

Table 2
Temperature difference, $T_W - T_0$, in K employed in experiments

$Re\backslash Ri$	6.5	13.2	27.4	42.7
300	0.5	1	2	3
500	1.4	2.8	5.6	8.4
700	2.7	5.4	10.9	16.3

the left wall). Measurements are taken at multiple x–y planes by traversing the light sheet and camera across the desired regions. The number of images that can be taken depends on the available PC RAM and the size of the frame acquired. In this case, it is limited to 180 full-size (12-bit) image pairs at a framing rate of 4 Hz. To make sure that the vortex dimensions are independent of the z-direction, the light sheet is adjusted to illuminate x–y regions at $z/H = 0.25$ and $z/H = 0.5$. A total of 900 pairs of images are acquired in each region for each of the z values. Velocity fields not satisfying a criterion of at least 95% successfully computed vectors are discarded. Rejected vectors are filled using a linear interpolation method based on the surrounding vectors. The mean velocity vectors for the longitudinal velocity component U and the transverse velocity component V are obtained by calculating statistics over all of the velocity vector maps.

For a Reynolds number of 300, the Richardson numbers are obtained for a temperature difference between the heated slab and the fluid of 0.5, 1, 2, and 3 K. The corresponding values of the Richardson numbers are $Ri = 6.5$ ($Gr = 5.85 \times 10^5$), 13.2 ($Gr = 1.188 \times 10^6$), 27.4 ($Gr = 2.466 \times 10^6$) and 42.7 ($Gr = 3.843 \times 10^6$), respectively. In order to study the influence of the Richardson number in the mean flow structure for different values of the Reynolds number, the values of the buoyancy parameter remain fixed. Therefore, for a Reynolds number of 500 and 700, the temperature difference between the fluid and the heated plate is obtained by using the fixed values of the Richardson numbers previously obtained. Table 2 shows the temperature difference for the assumed values of the Reynolds and Richardson numbers.

3. Results

The Flowmap System Hub stores 180 pairs of images in 45 s. Afterwards, the acquired images have to be transferred from the Flowmap System Hub to the PC before another set can be taken. Therefore, due to the fact that this mixed convection opposing flow is transient and the vortex presents longitudinal as well as transverse oscillations, it was impossible to match the mean flow statistics for all of the eight regions. Measurements are obtained at two positions related to the channel depth, at positions $z/H = 0.25$ and $z/H = 0.5$. The resulting flow structures for the employed Reynolds and Richardson numbers are almost the same, indicating that the flow can be considered as two-dimensional except at positions very close to the walls perpendicular to the heated plate. There is a critical Richardson (Grashof) number as a function of the Reynolds number where the vortex flow structure becomes unstable. The experimental measurements showed that for the range of Reynolds and Richardson (Grashof) numbers employed, the flow structures were always unstable, proving that those values were always above the critical Richardson (Grashof) values. Lower values of Ri could not be reached because of the lack of resolution in the measuring equipment for the temperature differences to be used. In the next subsections, the flow characteristics are analyzed for instantaneous and mean values. Instantaneous flow is displayed for certain time intervals of the experiment, while mean flow values are obtained by averaging all of the instantaneous images obtained for each experiment.

3.1. The instantaneous flow structure

The resulting flow produces a clockwise recirculation vortex due to the ascending heated fluid close to the heated slab and a descending cold forced flow away from the heated plate. This flow structure is unstable for the range of Reynolds and Richardson numbers used in the experiments. This subsection presents instantaneous flow images to illustrate how the vortex size and location varies in time and how longitudinal as well as transverse flow oscillations result in a displacement of the vortex center. The images displayed show how the flow structure has one or more vortexes and the way they interact. Fig. 3 shows the transient flow structure for a Reynolds number of *300* and a Richardson number of 13.2 ($Gr = 1.188 \times 10^6$), using frames with a time separation of 2 s between consecutive images. In this figure, the instantaneous streamlines are obtained for region 1, where the main vortex structure is located. An oscillating vortex fluctuates in the longitudinal and traverse direction (flapping). The frame sequence

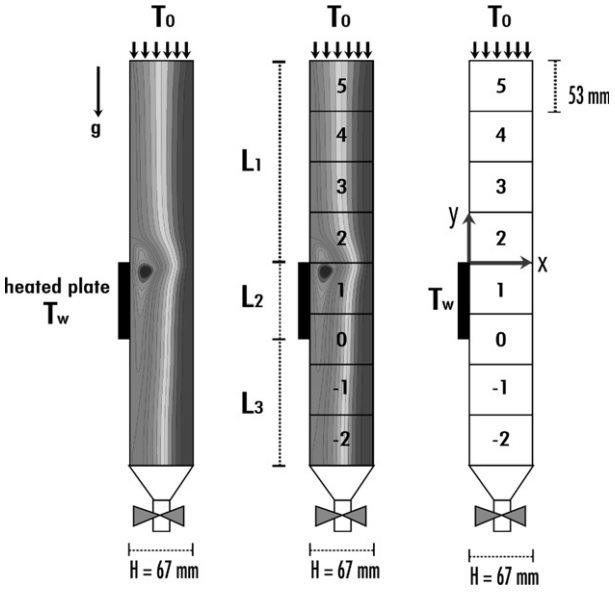

Fig. 2. Channel map regions.

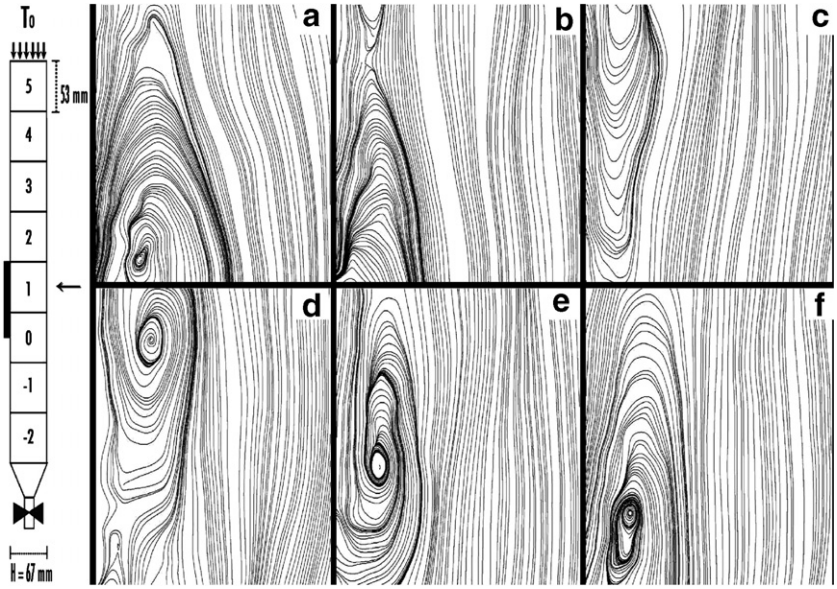

Fig. 3. Instantaneous flow for a Reynolds number of 300 and a Richardson number of 13.2 ($Gr = 1.188 \times 10^6$) in region 1 using frames with a time separation of 2 s.

shows that the longitudinal oscillation of the vortex structure results in a vortex displacement that travels from region 0 to region 2, thus producing both longitudinal and transverse flow oscillations. For a Reynolds number of 300, the flow structure shown in Fig. 3 has either one or two interacting vortexes. As can be seen, the frequency with which they pair is relatively large in comparison with that obtained for higher values of the Reynolds and Richardson numbers. For the image sequence shown in Fig. 3 it occurs only once in an interval of 6 s. Fig. 4 shows the transient vortical flow structure for a higher Reynolds number of 500 and a Richardson number of 27.4 ($Gr = 6.85 \times 10^6$), for region 3. In the present figure, less streamlines are displayed for the sake of clarity because the number of swinging vortexes interacting increased up to three. In this case, the interaction between one, two or three vortexes has a higher frequency.

Due to the fact that this opposed mixed convection flow is always transient for the given Reynolds and Richardson numbers employed, it is not possible to match all of the maps to obtain a single image encompassing all of the eight regions measured. It is then preferable to reduce the

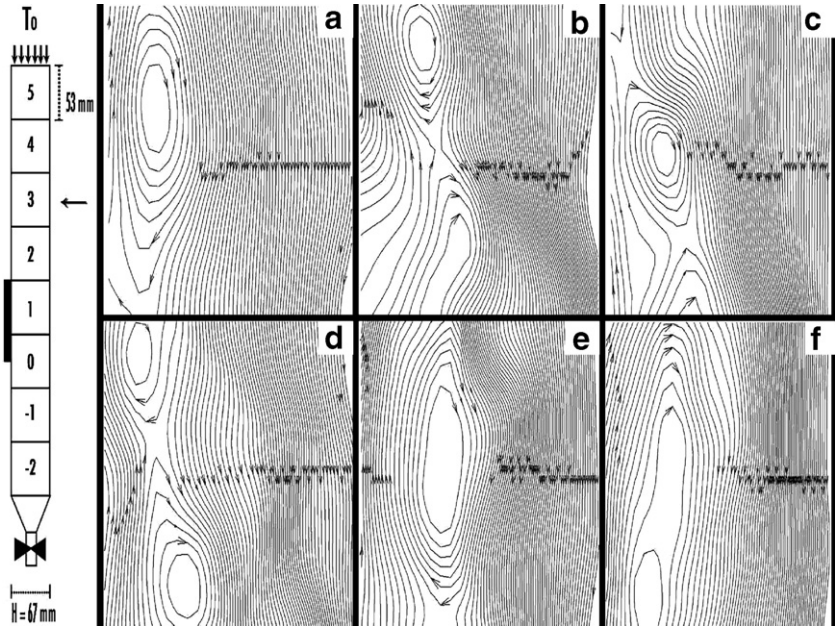

Fig. 4. Instantaneous flow for a Reynolds number of 500 and a Richardson number of 27.4 ($Gr = 6.85 \times 10^6$) in region 3 using frames with a time separation of 2 s.

problem by introducing a single parameter which characterizes the flow response. In order to study the flow oscillation, the mass flux centroid, x_p

$$x_p = \frac{\sum_{i=1}^{N} x_i u_i}{\sum_{i=1}^{N} u_i} \tag{1}$$

is obtained as a function of time, where x_i is the length from the heated wall to the node i, u_i is the longitudinal velocity associated to every node i and N corresponds to the total number of interrogation regions in the image (which in our case is $N = 20$). The lower section of region 1 is used as a reference location for measuring x_p. The time variations of this parameter are directly related to the transverse flow oscillations. The location of the mass flux centroid is displayed for an interval of $t_f = 45$ s, which is the time required to record 180 pairs of images. The elapsed time is normalized with the residence time H/U_0 and the mass flux centroid is normalized with the channel width.

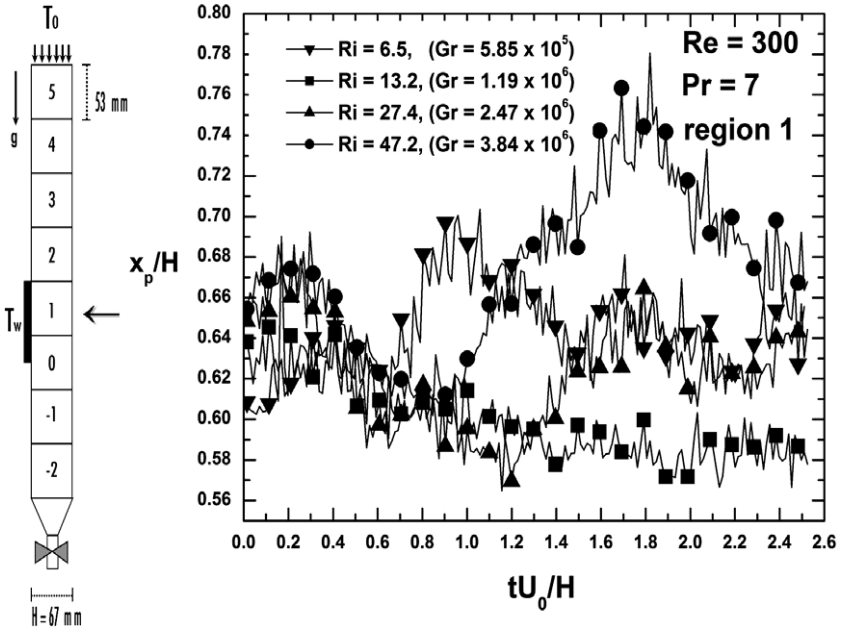

Fig. 5. Nondimensional mass flux centroid for a Reynolds number of 300.

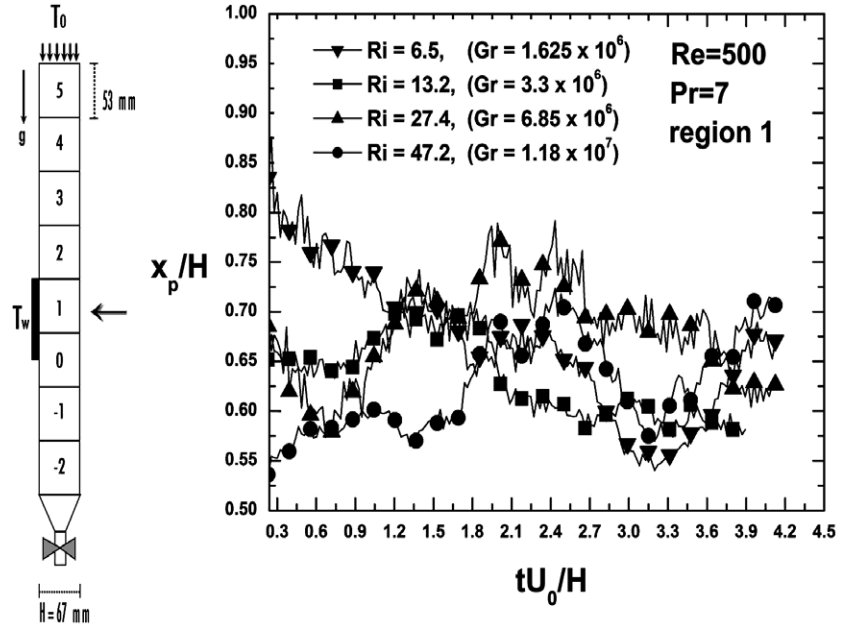

Fig. 6. Nondimensional mass flux centroid for a Reynolds number of 500.

Figs. 5–7 illustrate the mass flux oscillations as a function of the nondimensional time for three different values of the Reynolds number, 300, 500 and 700 and four different values of the buoyancy parameter. The important time response corresponds to the lower frequencies while the high frequencies could be associated to noise. Fig. 5 shows the corresponding values for a Reynolds number of 300. In this case, it was not possible to represent the time response for one cycle because of restrictions in the experimental equipment, where the maximum recording time was limited to 45 s, which is small compared with the residence time for low Reynolds numbers. As the Reynolds number increases

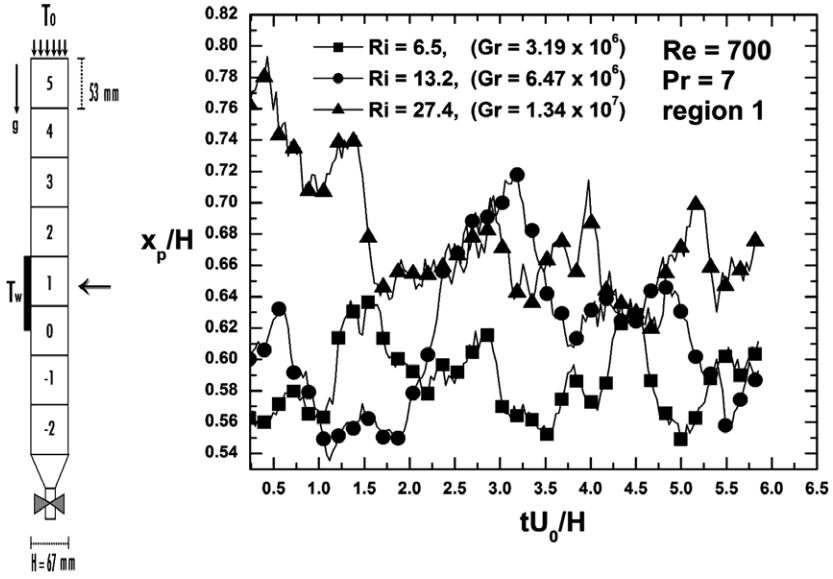

Fig. 7. Nondimensional mass flux centroid for a Reynolds number of 700.

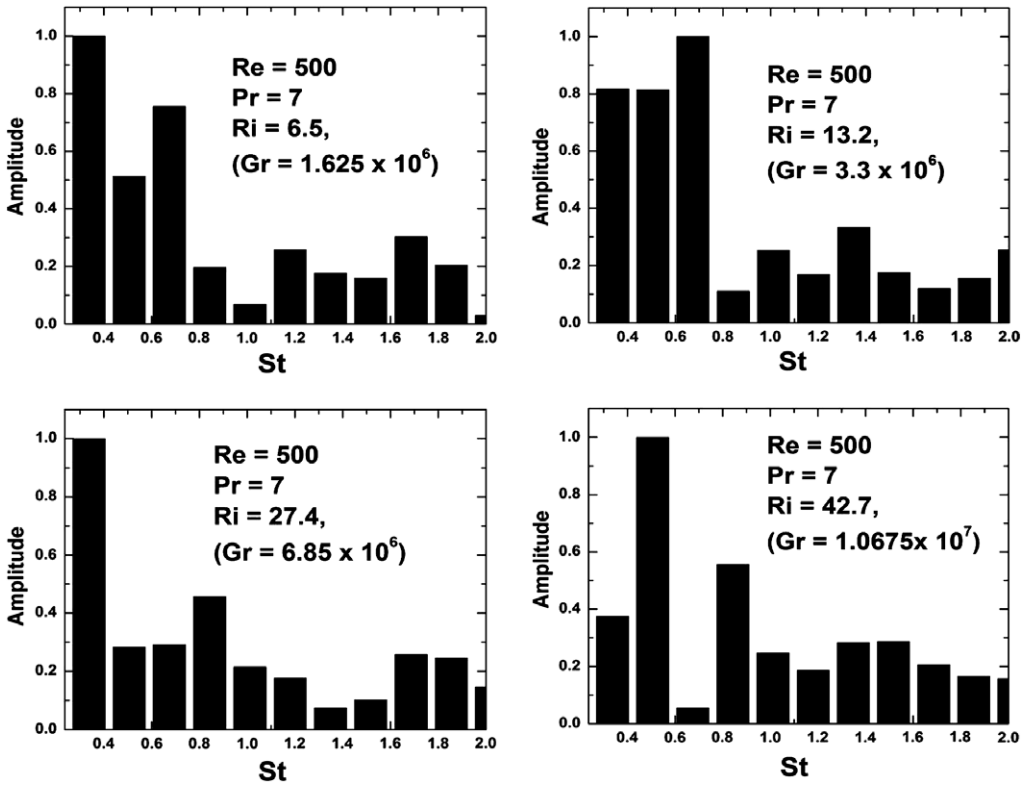

Fig. 8. Nondimensional oscillation frequencies ($St = fH/U_0$) for a Reynolds number of 500.

as shown in Figs. 6 and 7 for Reynolds numbers of 500 and 700, respectively, the low frequency response could be resolved. Figs. 8 and 9 show the normalized amplitude of the Fourier transform of the function $x_p(t\ U_0/H)$ for Reynolds numbers of 500 and 700 and different values of the buoyancy parameters as a function of the Strouhal number, $St = fH/U_0$, where f corresponds to the frequency in Hertz. Here, the Strouhal number relates the characteristic flow residence time, H/U_0 to the oscillation time. The infrared cut-off is dictated by the final measuring time, $St_{co} = (1/t_f)(H^2/v)(1/Re)$, where v corresponds to the kinematic viscosity of the fluid. For all cases studied, the max-

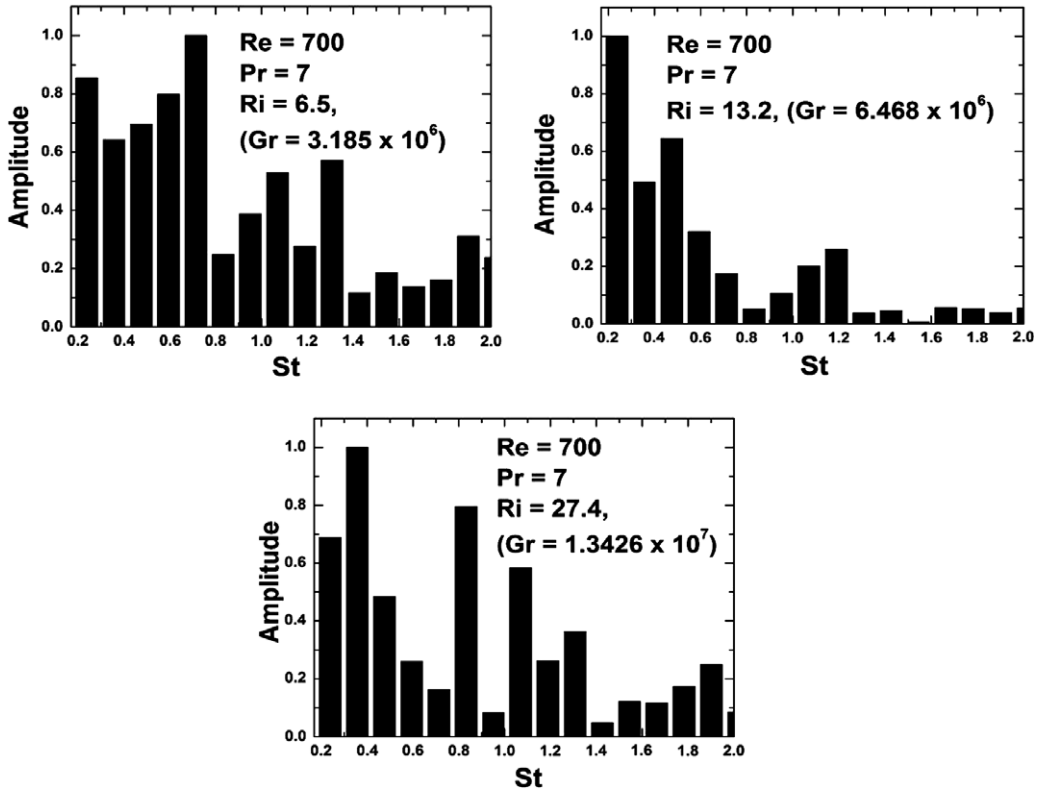

Fig. 9. Nondimensional oscillation frequencies ($St = fH/U_0$) for a Reynolds number of 700.

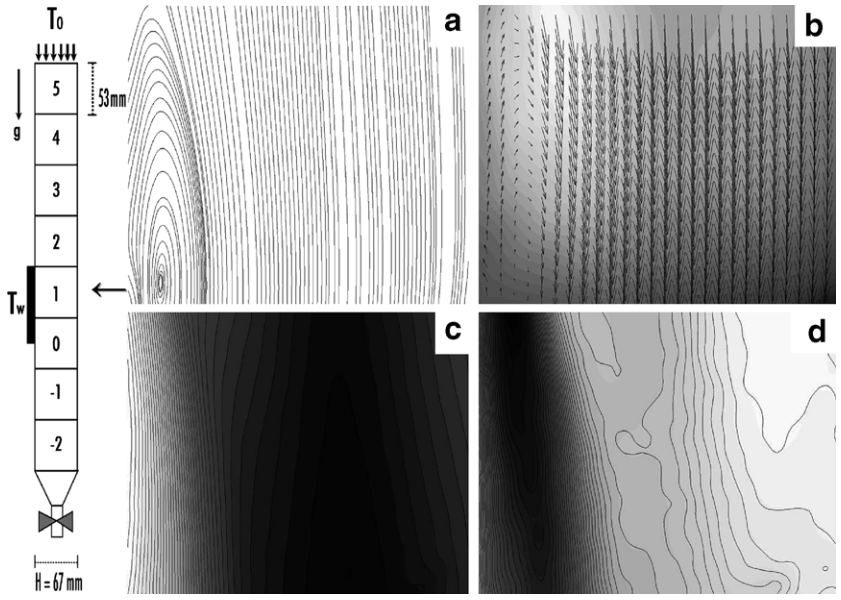

Fig. 10. Mean flow values at $Re = 300$ and $Ri = 6.5$ ($Gr = 5.85 \times 10^5$): (a) streamlines, (b) transverse velocity component and 2D vectors (c) longitudinal velocity and (d) vorticity.

imum amplitude occurs for low Strouhal numbers, close to the cut-off.

3.2. The mean flow structure

In this subsection, in an attempt to reduce the complexity of the experimental data in the resulting flow structure, the mean flow quantities in the x–y plane for $z = 0.5$ H (half of the channel depth) are presented. The mean values of the flow fields are obtained by averaging the instantaneous flow fields. A total of five sets were taken for each channel region. Each set is comprised of 180 pairs of images, and therefore, a total of 1800 images for each region were used to obtain the average flow. Figs. 10–13 show the resulting mean flow values for a Reynolds number of 300 and four different values of the Richardson (and Grashof) numbers: $Ri = 6.5$ ($Gr = 5.85 \times 10^5$), 13.2 ($Gr = 1.188 \times 10^6$), 27.4 ($Gr = 2.466 \times 10^6$) and 42.7 ($Gr = 3.843 \times 10^6$). The images displayed show that the flow structure presents one or more vortexes circulating in a clockwise direction. The location of the center of the vortex is obtained with the mean values and is strongly dependent on the Richardson (Grashof) numbers, shifting from region 1 to region 3 as the buoyancy parameter

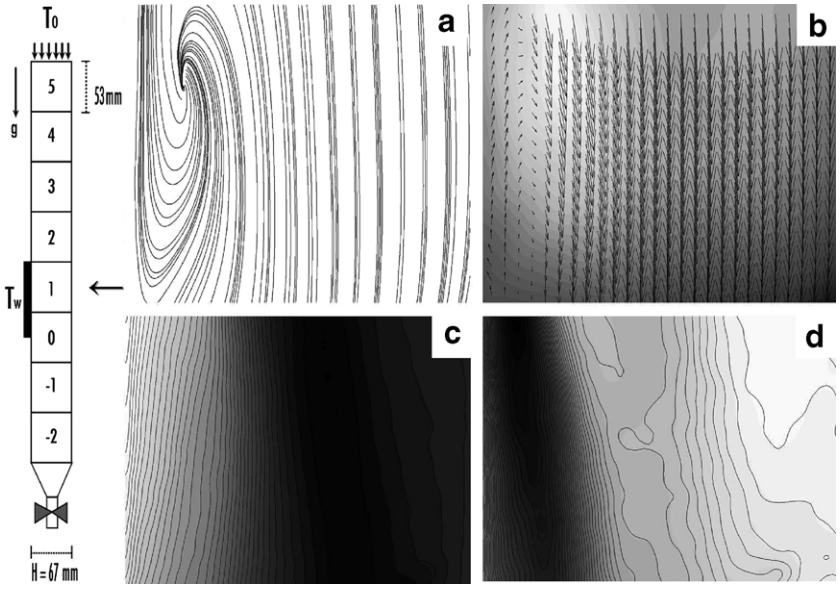

Fig. 11. Mean flow values at $Re = 300$ and $Ri = 13.2$ ($Gr = 1.188 \times 10^6$): (a) streamlines, (b) transverse velocity component and 2D vectors (c) longitudinal velocity and (d) vorticity.

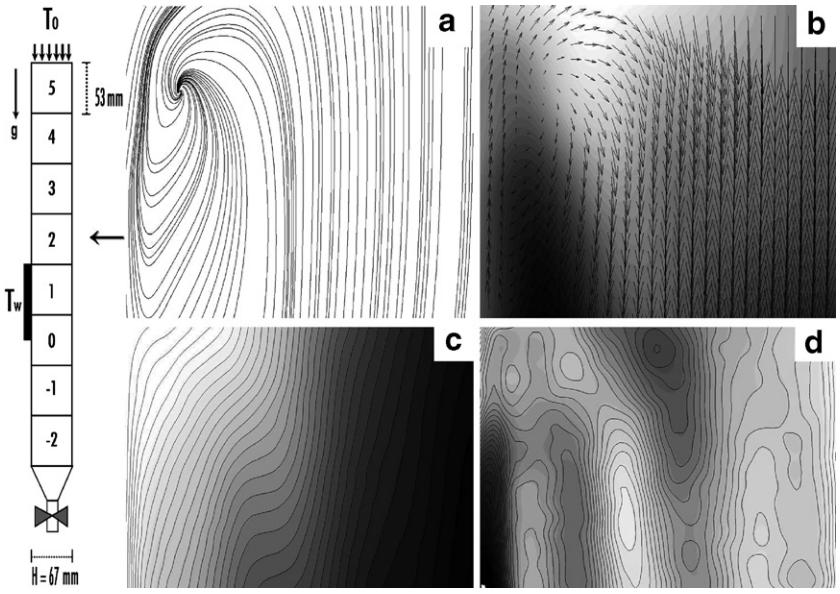

Fig. 12. Mean flow values at $Re = 300$ and $Ri = 27.4$ ($Gr = 2.466 \times 10^6$): (a) streamlines, (b) transverse velocity component and 2D vectors (c) longitudinal velocity and (d) vorticity.

increases. Fig. 10 shows the steady streamlines (a), the transverse velocity component together with the velocity vectors (b), the longitudinal velocity component (c) and the vorticity contours (d) in the x–y plane for region 1 for $Ri = 6.5$ ($Gr = 5.85 \times 10^5$). In this images, darker zones correspond to negative velocity and positive vorticity, while lighter zones correspond to positive velocity and negative vorticity. The plots shown in Figs. 10–15 are selected for the region where the center of the mean vortex structure is located. In the case where the flow structure has more than one vortex at the same time throughout the channel, the region chosen is the one in which the larger vortex is located. Fig. 11 shows the same plots for $Ri = 13.2$ ($Gr = 1.188 \times 10^6$) and also for region 1. Compared with the previous one, this figure shows how the center of the mean vortex has shifted up for this larger Richardson number. As the Richardson number increases, the center of the vortex continues to emigrate to higher regions of the channel as Figs. 12 and 13 show.

Figs. 12, 14 and 15 show the influence of the Reynolds number on the mean flow structure for a fixed Richardson number, $Ri = 27.4$. The thickness of the mean vortex struc-

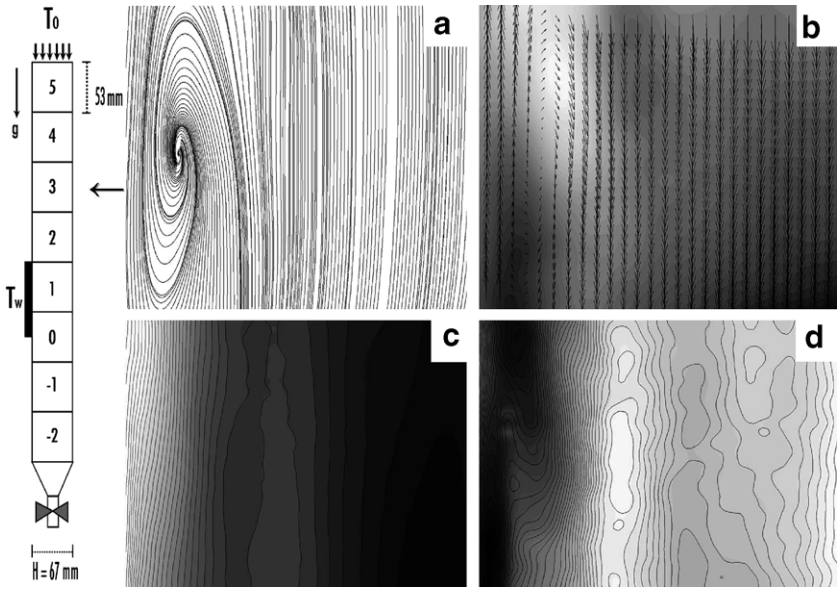

Fig. 13. Mean flow values at $Re = 300$ and $Ri = 42.7$ ($Gr = 3.843 \times 10^6$): (a) streamlines, (b) transverse velocity component and 2D vectors (c) longitudinal velocity and (d) vorticity.

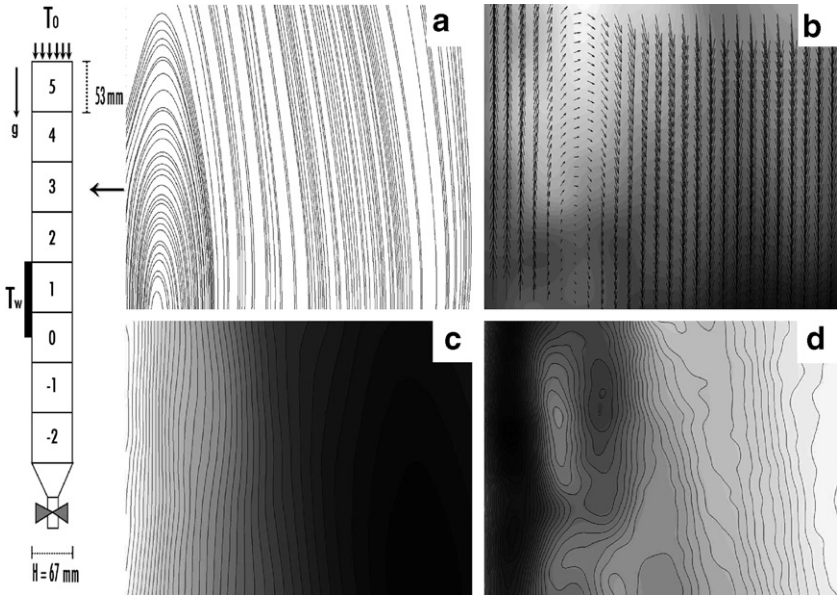

Fig. 14. Mean flow values at $Re = 500$ and $Ri = 27.4$ ($Gr = 6.85 \times 10^6$): (a) streamlines, (b) transverse velocity component and 2D vectors (c) longitudinal velocity and (d) vorticity.

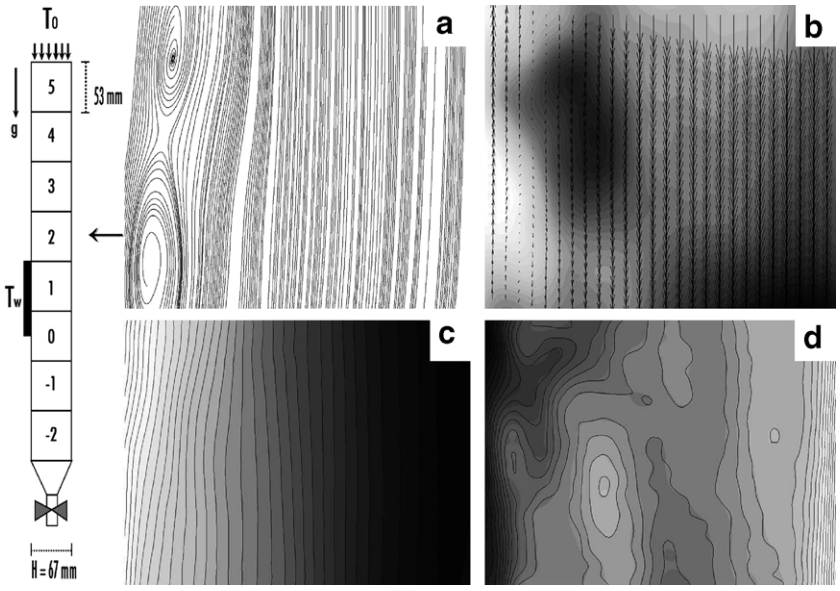

Fig. 15. Mean flow values at $Re = 700$ and $Ri = 27.4$ ($Gr = 13.426 \times 10^6$): (a) streamlines, (b) transverse velocity component and 2D vectors (c) longitudinal velocity and (d) vorticity.

ture decreases and its length increases by increasing the Reynolds number. For a Reynolds number of 700, multiple mean vortex structures appear as shown in Fig. 15. In Fig. 16, the overall mean vortex structure is assembled by patching the different regions obtained at different times, for a Reynolds number of 300 and two different Richardson numbers, $Ri = 6.5 (Gr = 5.85 \times 10^5)$ and 13.2 ($Gr = 1.188 \times 10^6$). The mean vortex dimensions are enhanced by increasing buoyancy. Fig. 17 shows the same behavior for a higher Reynolds number of $Re = 500$ and $Ri = 6.5$ ($Gr = 1.625 \times 10^5$) and 42.7 ($Gr = 10.675 \times 10^5$). The mean vortex dimensions increase with the Reynolds number for a fixed Richardson number. As a summary, Fig. 18 shows the mean vortex length and the mean vortex width related to the channel width H as a function of the Grashof (a and

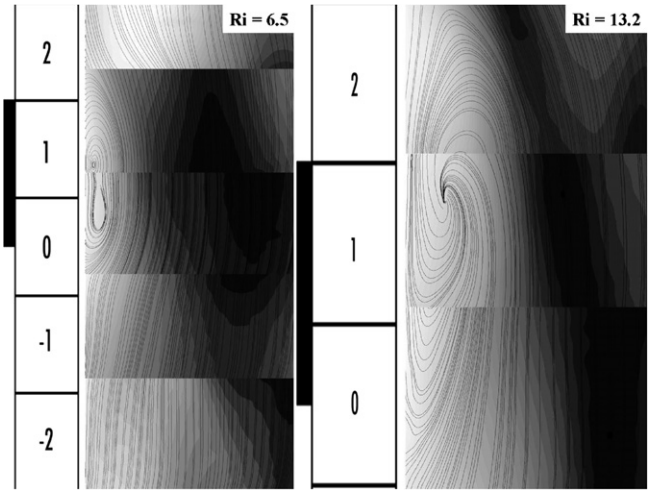

Fig. 16. Streamlines and longitudinal velocity mean flow values at $Re = 300$ for $Ri = 6.5$ ($Gr = 5.85 \times 10^5$) and $Ri = 13.2$ ($Gr = 1.188 \times 10^6$).

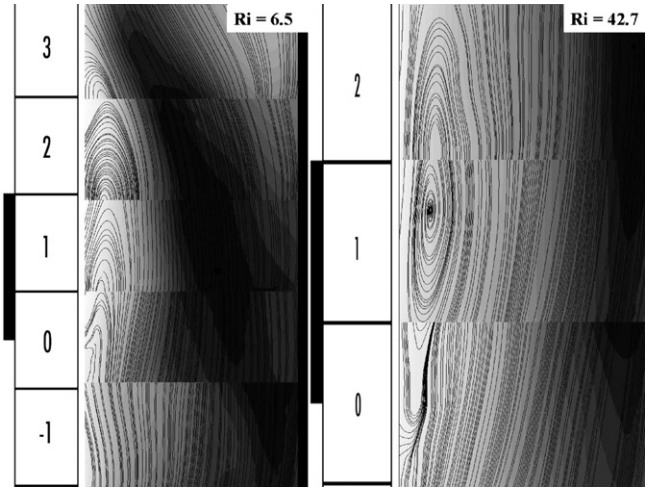

Fig. 17. Streamlines and longitudinal velocity mean flow values at $Re = 500$ for $Ri = 6.5$ ($Gr = 1.625 \times 10^6$) and $Ri = 42.7$ ($Gr = 10.675 \times 10^6$).

c) and Richardson (b and d) numbers for three different values of the Reynolds number. For the case where several vortex structures are present, the mean length of the vortex corresponds to the total length of the various vortex formations. The mean vortex length always increases for increasing values of the Grashof and Richardson numbers for all of the considered values of the Reynolds number. The vortex dimensions for a given Grashof number always decrease for increasing values of the Reynolds number (see Fig. 18a and c). However, Fig. 18b shows that the length of the vortex for a given Richardson number first increases with increasing Reynolds number from 300 to 500 and then decreases with increasing Reynolds number from 500 to 700. For a given Richardson number the vortical structure becomes thinner as the Reynolds number

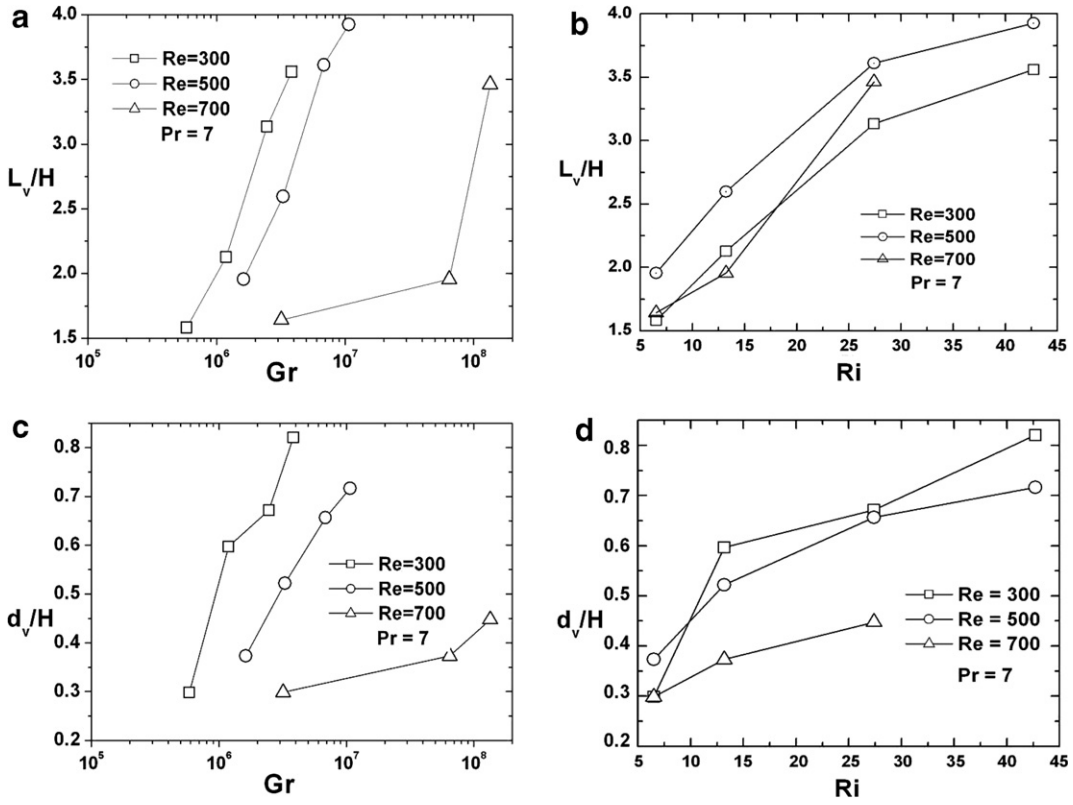

Fig. 18. Nondimensional vortex length and width as a function of the Grashof (a, c) and Richardson (b, d) numbers for three different values of the Reynolds number.

increases. Fig. 18 shows that the mean vortex dimensions are better represented by using the Grashof and Reynolds numbers as independent parameters.

4. Conclusions

In this paper, PIV measurements are reported for a transient, laminar, mixed convection flow due to a differential and asymmetric heating condition in a vertical channel with a square section when buoyancy opposes the gravity driven flow. A range of the Reynolds number (300–700) in combination with several values of the Richardson (6–42) or Grashof (10^6–10^8) numbers are studied in order to show how they affect the channel's flow structure. Buoyancy effects are larger adjacent to heated surfaces, generating an upward flow opposing the forced downward cool fluid flow. These highly unstable flow conditions generate a large vortex structure, which was always unsteady for the parameters employed in the experiments. For larger values of the Reynolds number, two or three small swinging vortexes coexisted producing a very complex flow structure. Instantaneous velocity measurements have been obtained for up to 45 s using the PIV technique. Flow oscillations were detected by using the mass flow centroid as a function of time in a selected position above the heated plate. The nondimensional oscillation frequency or Strouhal number has been obtained by using the Fourier transform of the mass flow centroid. The maximum amplitude of the Fourier transform occurs for Strouhal numbers close to the infrared cut-off, of order unity, indicating that the oscillation time is close to the residence time (time needed for the fluid to travel a distance H with the inflow velocity U_0). From the instantaneous velocity measurements, the averaged velocity field has been obtained and the mean vortex dimensions were deduced for different Reynolds and Grashof numbers. For a given Grashof number, the vortex becomes thinner and shorter as the Reynolds number increases, and for a given Reynolds number, the vortex structure becomes larger and thicker as the Grashof (Richardson) increases. A better representation is obtained when using the Reynolds and Grashof numbers as independent parameters.

Acknowledgement

This work has been supported by DGAPA of UNAM, under Contract IN-1114505.

References

[1] J.P. Hartnett, M. Kostic, Heat transfer to Newtonian and non-Newtonian fluids in rectangular ducts, Advances in Heat Transfer 19 (1989) 247–356.

[2] W. Aung, G. Worku, Theory of fully developed, combined convection including flow reversal, Journal of Heat Transfer 108 (1986) 485–488.

[3] W. Aung, G. Worku, Developing flow and flow reversal in a vertical channel with asymmetric wall temperatures, ASME Journal of Heat Transfer 108 (1986) 299–304.
[4] D. Ingham, D. Keen, P. Heggs, Two-dimensional combined convection in vertical parallel plate ducts including situations of flow reversal, International Journal for Numerical Methods in Engineering 26 (1988) 1645–1664.
[5] G. Evans, R. Greif, Buoyant instabilities in downward flow in a symmetrically heated vertical channel, International Journal of Heat and Mass Transfer 40 (10) (1997) 2419–2430.
[6] T. Lin, C. Yin, W. Yan, Transient laminar mixed convective heat transfer in a vertical flat duct, ASME Journal of Heat Transfer 113 (1991) 384–390.
[7] L.S. Yao, Free and forced convection in the entry region of a heated vertical channel, International Journal of Heat and Mass Transfer 26 (1) (1983) 65–72.
[8] T.-S. Chang, T.-F. Lin, Steady and oscillatory opposing mixed convection in a simmetrically heated vertical channel with a low-prandtl number fluid, International Journal of Heat and Mass Transfer 36 (15) (1993) 3783–3795.
[9] D. Elpidorou, V. Prasad, V. Modi, Convection in a vertical channel with a finite wall heat source, International Journal of Heat and Mass Transfer 34 (2) (1991) 573–578.
[10] T. Lin, T. Chang, Y. Cheng, Development of oscillatory asymmetric recirculating flow in transient laminar opposing mixed convection in a symmetrically heated vertical channel, ASME Journal of Heat and Transfer 115 (1993) 342–352.
[11] E.M. Sparrow, G.M. Chrysler, L.F. Azevedo, Conjugate natural convection from a vertical heated slab, International Journal of Heat and Mass Transfer 106 (1984) 325–332.
[12] X. Zhang, S. Dutta, Heat transfer analysis of buoyancy-assisted mixed convection with asymmetric heating conditions, International Journal of Heat and Mass Transfer 41 (1998) 3255–3264.
[13] C.F. Odouza, A.A. Wragg, M.A. Patrick, Mixed convection mass transfer studies of opposing and aiding flow in a parallel plate, Journal of Applied Electrochemistry 28 (1998) 697–702.
[14] S. Kimura, A. Okajima, T. Kiwata, Conjugate natural convection from a vertical heated slab, International Journal of Heat and Mass Transfer 41 (1998) 3203–3211.
[15] H.I. Abu-Mulaweh, Measurements of laminar mixed convection flow adjacent to an incluined surface with uniform wall heat flux, International Journal of Thermal Sciences 42 (2003) 57–62.
[16] C. Gau, K.A. Yih, W. Aung, Reversed flow structure and heat transfer measurements for buoyancy-assisted convection in a heated vertical duct, ASME Journal of Heat Transfer 114 (1992) 928–935.
[17] R.A. Wirtz, R.J. Stutzman, Experiments on free convection between vertical plates with symmetric heating, ASME Journal of Heat Transfer 104 (1982) 501–507.
[18] R. Moffat, Describing the uncertainties in experimental results, Experimental Thermal and Fluid Science 1 (1988) 3–17.